



ATLAS Note

GROUP-2017-XX

14th January 2020



Draft version 0.1

1

2

Search for the Effects of Dimension-six

3

Operators in the interactions of the Higgs

4

Boson with the Top Quark

5

The ATLAS Collaboration

6 Several theories Beyond the Standard Model modify the A differential measurement of the
7 Higgs transverse momentum spectrum is performed for events where the Higgs Boson is
8 produced from top quark pairs and decays to final states that include multiple leptons. A
9 two-bin fit is used. The channels considered include two same-sign lepton and three lepton
10 final states. An effective field theory approach is used to parameterize and place limits on the
11 strength of potential six-dimensional operators.

© 2020 CERN for the benefit of the ATLAS Collaboration.

12 Reproduction of this article or parts of it is allowed as specified in the CC-BY-4.0 license.

13	Contents	
14	I Introduction	5
15	1 Introduction	5
16	II Theoretical Motivation	7
17	2 The Standard Model and the Higgs Boson	7
18	2.1 The Forces and Particles of the Standard Model	7
19	2.2 The Higgs Mechanism	10
20	2.2.1 The Higgs Field	10
21	2.2.2 Electroweak Symmetry Breaking	12
22	2.3 Limitations of the Standard Model	15
23	3 Effective Field Theory in $t\bar{t}H$ Production	15
24	3.1 Extensions to the Higgs Sector	16
25	3.2 Six Dimensional Operators	16
26	III The LHC and the ATLAS Detector	16
27	4 The LHC	16
28	5 The ATLAS Detector	19
29	5.1 Inner Detector	21
30	5.2 Calorimeters	21
31	5.3 Muon Spectrometer	23
32	5.4 Forward Detector	24
33	5.5 Trigger System	24
34	IV Search for Dimension-Six Operators	25
35	6 Data and Monte Carlo Samples	25
36	7 Object Reconstruction	25
37	8 Higgs Momentum Reconstruction	26
38	8.1 Truth Level Reconstruction	27
39	8.2 b-jet Identification	27
40	8.3 Higgs Reconstruction	27
41	8.4 p_T Prediction	27

42	9 Signal Region Definitions	27
43	9.1 2lSS	27
44	9.2 3l	27
45	10 Background Rejection MVA	27
46	10.1 2lSS	30
47	10.1.1 2lSS - High p_T	30
48	10.1.2 2lSS - Low p_T	30
49	10.2 3l Semi-Leptonic	30
50	10.2.1 3l Semi-Leptonic - High p_T	30
51	10.2.2 3l Semi-Leptonic - Low p_T	30
52	10.3 3l Fully Leptonic	30
53	10.3.1 3l Fully Leptonic - High p_T	30
54	10.3.2 3l Fully Leptonic - Low p_T	30
55	11 Systematic Uncertainties	30
56	12 Results	32
57	V Conclusion	32
58	Appendices	34

Part I

Introduction

1 Introduction

Particle physics is an attempt to describe the fundamental building blocks of the universe and their interactions, and the Standard Model (SM) - our best current theory of fundamental particle physics - does a remarkable job of doing exactly that. All known fundamental particles and (almost) all of the forces underlying their interactions can be explained by the SM, and the predictions from this theory agree with experiment to an incredibly precise degree. This is especially true since the Higgs Boson, last piece of the SM predicted decades before, was finally discovered at the Large Hadron Collider (LHC) in 2012.

Despite the success of the SM, there remains significant work to be done. For one, the SM is incomplete: it fails to explain gravity at the quantum scale, to give any explanation for the observation of Dark Matter, or to provide a mechanism for neutrinos to gain mass. A Higgs Boson with a mass of around 125 GeV also gives rise to what is known as a hierarchy problem - such a low mass Higgs requires a seemingly unnatural level of “fine tuning”.

A promising avenue for addressing these problems is to study the properties of the Higgs Boson and the way it interacts with other particles, in part because these interactions have not been accurately measured before. This leaves the Higgs sector of the SM a fertile ground to

search for new physics. Its interactions with the Top Quark are a particularly promising place to look: The Higgs Boson is responsible for giving particles their mass, and the strength of a particle's interaction with the Higgs is proportional to its mass. As the most massive of the fundamental particles, the Top Quark has the strongest coupling to the Higgs Boson. This means any new physics in the Higgs sector is likely to present itself most prominently in its interaction with the Top Quark.

These interactions can be measured by directly by studying the production of a Higgs Boson in association with a pair of Top Quarks ($t\bar{t}H$). While studies have been done measuring the overall rate $t\bar{t}H$ of production, there are several theories of physics Beyond the Standard Model (BSM) that would affect the kinematics of $t\bar{t}H$ production without affecting its overall rate. This dissertation attempts to make a differential measurement on the kinematics of $t\bar{t}H$ production in order to search for these BSM effects.

The proton-proton collision data collected by the ATLAS detector at the LHC from 2015-2018 provides the opportunity to made such a measurement for the first time. The unprecedented energy acheived by the LHC during this period greatly increase the rate at which $t\bar{t}H$ events are produced, and the large amount of data collected allow a differential measurement to be performed.

This dissertation begins with a brief explanation of the SM, its limitations, and the theoretical motivation behind this work. This is followed by a description of the LHC and the ATLAS detector. The analysis strategy is then described, and the results are presented. Finally, the results

97 of the study are summarized in the conclusion.

98 **Part II**

99 **Theoretical Motivation**

100 **2 The Standard Model and the Higgs Boson**

101 The Standard Model of particle physics (SM) is a Quantum Field Theory (QFT) describing the
102 known fundamental particles and their interactions. It accounts for three of the four known
103 fundamental force - electromagnetism, the weak nuclear force, and the strong nuclear force, but
104 not gravity. Further, the SM describes a mechanism for combining the weak and electromagnetic
105 forces into a singular interaction, known as the electroweak force. It is a non-Abelian gauge
106 theory, invariant under the Lie Group $SU(3)_C \otimes SU(2)_L \otimes U(1)_Y$, where C refers to color
107 charge, L, the helicity of the particle, and Y, the hypercharge.

108 **2.1 The Forces and Particles of the Standard Model**

109 The SM particles, summarized in figure [2.1](#), can be classified into two general categories based
110 on their spin: fermions, and bosons.

Standard Model of Elementary Particles

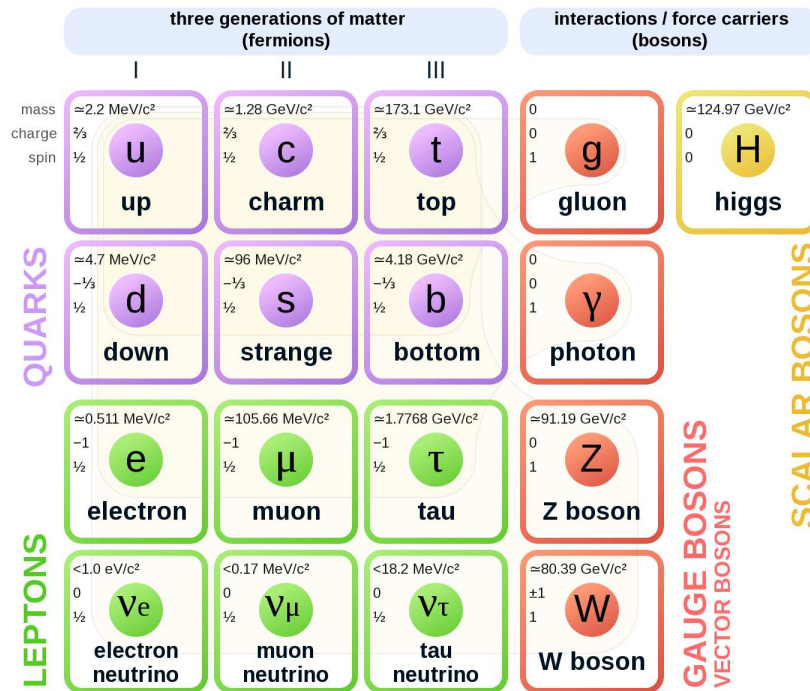


Figure 2.1: A summary of the particles of the Standard Model, including their mass, charge and spin, with the fermions listed on the left, and the bosons on the right. []

111 Fermions are particles with $\frac{1}{2}$ -integer spin, which according to the spin-statistics theorem,
 112 causes them to comply with the Pauli-exclusion principle []. They can be separated into two
 113 groups, leptons and quarks, each of which consist of three generations of particles with increasing
 114 mass.

115 Leptons are fermions interact via the electroweak force, but not the strong force. The three
 116 generation of leptons consist of the electron and electron neutrino, the muon and muon neutrino,
 117 the tau and tau neutrino. The quarks, which do interact via the strong force - which is to say they
 118 have color charge - in addition to the electroweak force. The three generations include the up

119 and down quarks, the strange and charm quarks, and the top and bottom quarks. Each of these
 120 generations form left-handed doublets invariant under $SU(2)$ transformations. For the leptons
 121 these doublets are:

$$\begin{pmatrix} e^- \\ \nu_e \end{pmatrix}_L, \begin{pmatrix} \mu^- \\ \nu_\mu \end{pmatrix}_L, \begin{pmatrix} \tau^- \\ \nu_\tau \end{pmatrix}_L \quad (2.1)$$

122 And for the quarks:

$$\begin{pmatrix} u \\ d \end{pmatrix}_L, \begin{pmatrix} s \\ c \end{pmatrix}_L, \begin{pmatrix} t \\ b \end{pmatrix}_L \quad (2.2)$$

123 For both leptons and quarks, the heavier generations can decay into the lighter generation
 124 of particles, while the first generation does not decay. Hence, ordinary matter generally consists
 125 of this first generation of fermions - electrons, up quarks, and down quarks. Each of these
 126 fermions has a corresponding anti-particle, which has an equal mass as its partner but opposite
 127 charge. The fermions acquire their mass via the Higgs Mechanism, except for the neutrinos,
 128 whose mass has been experimentally confirmed but is not accounted for in the SM.

129 Bosons, by contrast, have integer spin, and are therefore unconstrained by the Pauli-
 130 exclusion principle. The SM includes two kinds of bosons: Gauge bosons, which are spin-1
 131 particles that mediate the interactions between the fermions, and a single scalar, i.e. spin-0,
 132 particle - the Higgs Boson. Of the gauge bosons, the W^+ , W^- and Z bosons - which are the

133 mass eigenstates of the electroweak bosons - mediate the weak interaction, while the photon
 134 mediates the electric force, and the gluon mediates the strong force.

135 2.2 The Higgs Mechanism

136 A key feature of the SM is the gauge invariance of its Lagrangian. However, any terms added to
 137 the Lagrangian giving mass to the gauge bosons would violate the underlying symmetry of
 138 the theory. This presents a clear problem with the theory: The experimental observation that the
 139 W and Z bosons have mass seems to contradict the basic structure of the SM.

140 Rather than abandoning gauge invariance, an alternative way for particles to acquire mass
 141 beyond adding a simple mass term to the Lagrangian was theorized by Higgs, Englert and Brout
 142 in 1964 []. This procedure for introducing masses for the gauge bosons while preserving local
 143 gauge invariance, known as the Higgs mechanism, was incorporated into the electroweak theory
 144 by Weinberg in 1967 [].

145 2.2.1 The Higgs Field

146 The Higgs mechanism introduces a complex scalar SU(2) doublet, Φ , with the form:

$$\Phi = \begin{pmatrix} \phi^+ \\ \phi^0 \end{pmatrix}_L \quad (2.3)$$

147

This field introduces a scalar potential to the Lagrangian of the form:

$$V(\Phi) = \mu^2 |\Phi^\dagger \Phi| + \lambda (|\Phi^\dagger \Phi|)^2 \quad (2.4)$$

148

Where μ and λ are free parameters of the new field. This represents the most general

149

potential allowed while preserving $SU(2)_L$ invariance and renormalizability. In the case that

150

$\mu^2 < 0$, this potential takes the form shown in figure 2.2.

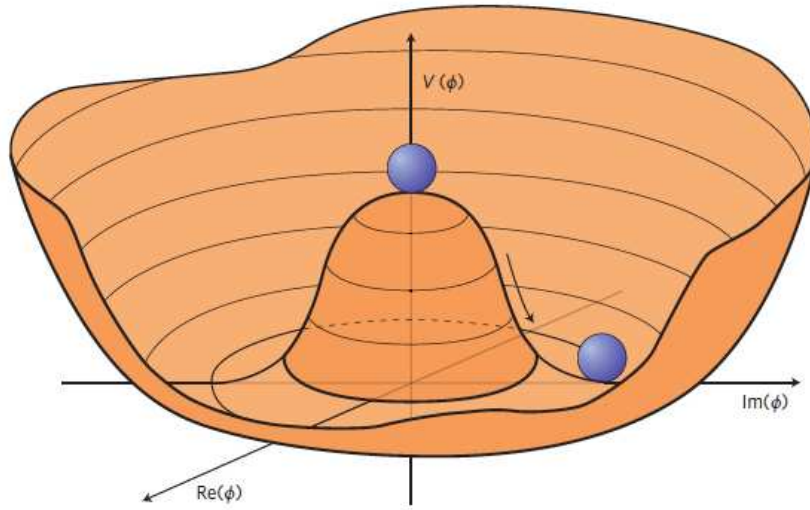


Figure 2.2: The value of the Higgs potential, $V(\Phi)$ as a function of Φ , for the case that $\mu^2 < 0$ [].

151

The significant feature of this potential is that its minimum does not occur for a value of

152

$\Phi = 0$. Instead, it is minimized when $|\Phi^\dagger \Phi| = -\mu^2/\lambda$. This means that in its ground state, the

153

Higgs field takes on a non-zero value - referred to as a vacuum expectation value (VEV). So while

154

the Higgs potential is globally symmetric, about the minimum this symmetry is broken. Since

155

the minimum is determined only by $\Phi^\dagger \Phi$, there is some ambiguity in the particular definition of

156 the VEV, but it is generally represented as

$$\langle \Phi \rangle = \frac{1}{\sqrt{2}} \begin{pmatrix} 0 \\ v \end{pmatrix} \quad (2.5)$$

157 The full value of Φ can be written as

$$\langle \Phi \rangle = \frac{1}{\sqrt{2}} \begin{pmatrix} 0 \\ v + H/\sqrt{2} \end{pmatrix} \quad (2.6)$$

158 with v being the value of the VEV, and H being the real value of the scalar field.

159 2.2.2 Electroweak Symmetry Breaking

160 The Electroweak (EWK) interaction is described in the SM by a $SU(2)_L \otimes U(1)_Y$ gauge theory.

161 This theory predicts three $SU(2)_L$ gauge boson, W_μ^1 , W_μ^2 , W_μ^3 , and a single $U(1)_Y$ gauge boson,

162 B_μ . The couplings of these bosons to the Higgs field show up in the kinetic terms of the scalar

163 field Φ in the Lagrangian:

$$(D_\mu \Phi)^\dagger (D^\mu \Phi) = |(\partial_\mu - \frac{ig}{2} W_\mu^a \sigma^a - \frac{ig'}{2} B_\mu Y) \Phi|^2 \quad (2.7)$$

Here D_μ represents the covariant derivative required to preserve gauge invariance, g and g' represent coupling constant of the gauge bosons, σ^a denotes the Pauli matrices of $SU(2)$, and Y represents the hypercharge of $U(1)$. The terms in this interaction which contribute to the masses of the gauge bosons can be written as:

$$\frac{1}{2}(0, v) \left(\frac{g}{2} W_\mu^a \sigma^a - \frac{g'}{2} B_\mu \right)^2 \begin{pmatrix} 0 \\ v \end{pmatrix} \quad (2.8)$$

Expanding these terms into the mass eigenstates of the electroweak interaction yields four physical gauge bosons, two charged and two neutral, which are linear combinations of the fields $W_\mu^1, W_\mu^2, W_\mu^3$, and B_μ :

$$\begin{aligned} W_\mu^\pm &= \frac{1}{\sqrt{2}} (W_\mu^1 \pm i W_\mu^2) \\ Z^\mu &= \frac{1}{\sqrt{(g^2 + g'^2)}} (-g' B_\mu + g W_\mu^3) \\ A^\mu &= \frac{1}{\sqrt{(g^2 + g'^2)}} (g B_\mu + g' W_\mu^3) \end{aligned} \quad (2.9)$$

And the masses of these fields are given by:

$$\begin{aligned} M_W^2 &= \frac{1}{4} g^2 v^2 \\ M_Z^2 &= \frac{1}{4} (g^2 + g'^2) v^2 \\ M_A^2 &= 0 \end{aligned} \quad (2.10)$$

172 This produces exactly the particles we observe - three massive gauge bosons and a single
 173 massless photon. The massless photon represents the portion of the gauge symmetry, a single
 174 $U(1)$ of the electromagnetic force, that remains unbroken by the VEV.

175 Interactions with the Higgs field also lead to the generation of the fermion masses, which
 176 in the Lagrangian take the form:

$$-\lambda_\psi(\bar{\psi}_L\phi\psi_R + \bar{\psi}_R\phi^\dagger\psi_L) \quad (2.11)$$

177 After symmetry breaking has occurred and ϕ has taken on the value of the VEV as written
 178 in equation 2.5, the mass terms for the fermions become $\lambda_\psi v$. Written this way, the fermion
 179 masses are proportional to their Yukawa coupling to the VEV, λ_ψ .

180 Based on the equation 2.6, an additional mass term, $\mu^2 H^2$ arises from the potential $V(\Phi)$.
 181 This term can be understood as an excitation of the Higgs field, a scalar boson with mass $M_H = \mu$.
 182 This is the Higgs boson, which comes about as a natural prediction of electroweak symmetry
 183 breaking.

184 The fermion's Yukawa coupling to the VEV take the same form as the fermion's coupling
 185 to the Higgs boson - λ_ψ . Therefore, the strength of a fermion's interaction with the Higgs is
 186 directly proportional to its mass. We now have a model that predicts a Higgs boson with mass
 187 $M_H = \mu$, which interacts with the fermions with coupling strength λ_ψ . Because μ and λ_ψ are

188 free parameters of the theory, the mass of the Higgs boson and its interactions with the fermions
 189 must be measured experimentally.

190 2.3 Limitations of the Standard Model

191 While the SM has great predictive power, there are still several experimental observation that the
 192 SM fails to explain. For example,

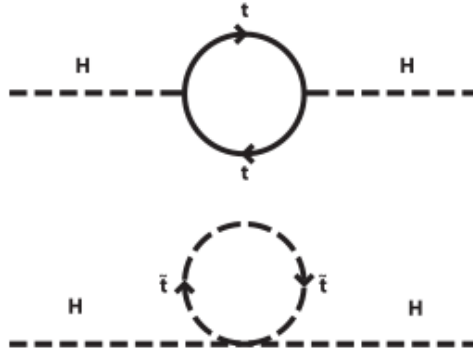


Figure 2.3: Above diagram is the leading order correction to the Higgs mass via a top quark loop, and below is the stop squark loop, coming from a supersymmetric extension of the SM, that provides a potential cancellation of the top diagram [1].

193 3 Effective Field Theory in $t\bar{t}H$ Production

194 Higher dimension operators are a common way to paramaterize the effects of physics at very
 195 high energies into

3.1 Extensions to the Higgs Sector

3.2 Six Dimensional Operators

While the SM has been tested to great precision, particularly at the LHC, it is generally accepted that it is only valid up to a certain energy scale. It is assumed that above a certain energy, at the scale where something like a Grand Unified Theory (GUT) or quantum gravity become relevant, the SM will not be applicable.

Part III

The LHC and the ATLAS Detector

4 The LHC

The Large Hadron Collider (LHC) is a particle accelerator consisting of a 27 km ring, designed to collide protons at high energy. Located outside of Geneva, Switzerland and buried about 100 m underground, it consists of a ring of superconducting magnets which are used to accelerate opposing beams of protons - or lead ions - which collide at the center of one of the various detectors located around the LHC ring which record the result of these collisions. These detectors include two general purpose detectors, ATLAS and CMS, which are designed to make precision measurements of a broad range of physics phenomenon, and two more specialized

212 experiments, LHCb and ALICE, which are optimized to study b-quarks and heavy-ion physics,
213 respectively.

214 The LHC first began running in 2009 at a proton-proton center of mass energy of $\sqrt{s} = 8$
215 TeV. It operated at this energy from 2009 to 2012, known as Run 1, and data collected during
216 this period was used in discovering the Higgs Boson. The LHC began running again in 2015,
217 and collected data at an increased energy of $\sqrt{s} = 13$ TeV until 2018, a period referred to as Run
218 2.

219 The LHC consists of a chain of accelerators, which accelerate the protons to higher and
220 higher energies until they are injected into the main ring. This process is summarized in figure
221 4.1. Protons extracted from a tank of ionized hydrogen are fed into a linear accelerator, LINAC2,
222 where they reach an energy of 50 MeV. From there, they enter a series of three separate circular
223 accelerators, before being injected into the main accelerator ring at an energy of 450 GeV. Within
224 the main ring protons are separated into two separate beams moving in opposite directions,
225 and their energy is increased to their full collision energy. Radiofrequency cavities are used to
226 accelerate these particles and sort them into bunches. From 2015-2018, these bunches consisted
227 of around 100 billion protons each with an energy of 6.5 TeV per proton, which collided at a rate
228 of 40 MHz, or every 25 ns.

229 Because these proton bunches consist of a large number of particles, each bunch crossing
230 consists of not just one, but several direct proton-proton collisions. The number of interactions
231 that occur per bunch crossing, μ , is known as pileup. During Run 2, the average pileup for bunch

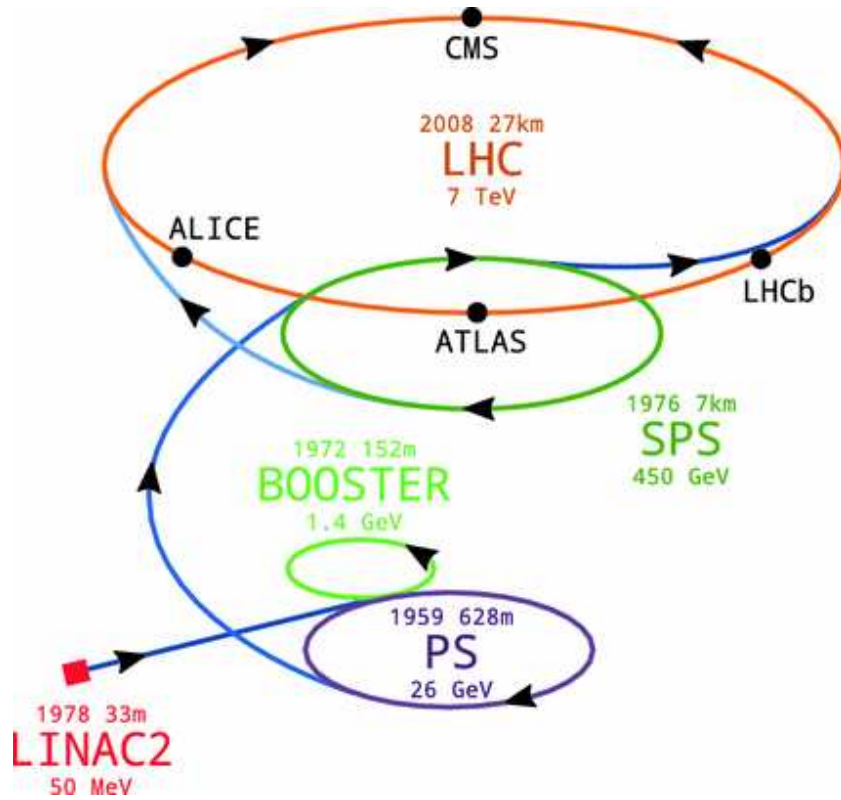


Figure 4.1: A summary of the accelerator chain used to feed protons into the LHC [1].

crossings was around $\langle \mu \rangle = 35$, with values typically ranging between 10 and 70.

The amount of data collected by the LHC is measured in terms of luminosity, which is the ratio of the number of events detected per unit time, $\frac{dN}{dt}$, and the interaction cross-section, σ .

$$\mathcal{L} = \frac{1}{\sigma} \frac{dN}{dt} \quad (4.1)$$

The design luminosity of the LHC is $10^{34} \text{cm}^{-2} \text{s}^{-1}$, however the LHC has achieved a luminosity of over $2 \times 10^{34} \text{cm}^{-2} \text{s}^{-1}$. The total luminosity is then this instantaneous luminosity

237 integrated over time.

$$\mathcal{L}_{\text{int}} = \int \mathcal{L} dt \quad (4.2)$$

238 The integrated luminosity collected by the ATLAS detector as of the end of 2018 is around
239 140 fb^{-1} , exceeding the expected integrated luminosity of 100 fb^{-1} .

240 **5 The ATLAS Detector**

241 ATLAS (a not terribly natural acronym for “A Toroidal LHC Apparatus”) is a general purpose
242 detector designed to maximize the detection efficiency of all physics objects, including leptons,
243 jets, and photons. This means it is capable of measuring all SM particles, with the exception of
244 neutrinos, the presence of which can be inferred based on missing transverse momentum. The
245 detector measures 44 m long, and 25 m tall.

246 The ATLAS detector consists of multiple layers, each of which serves a different purpose
247 in reconstructing collisions. At the very center of the detector is the interaction point where the
248 proton beams of the LHC collide.

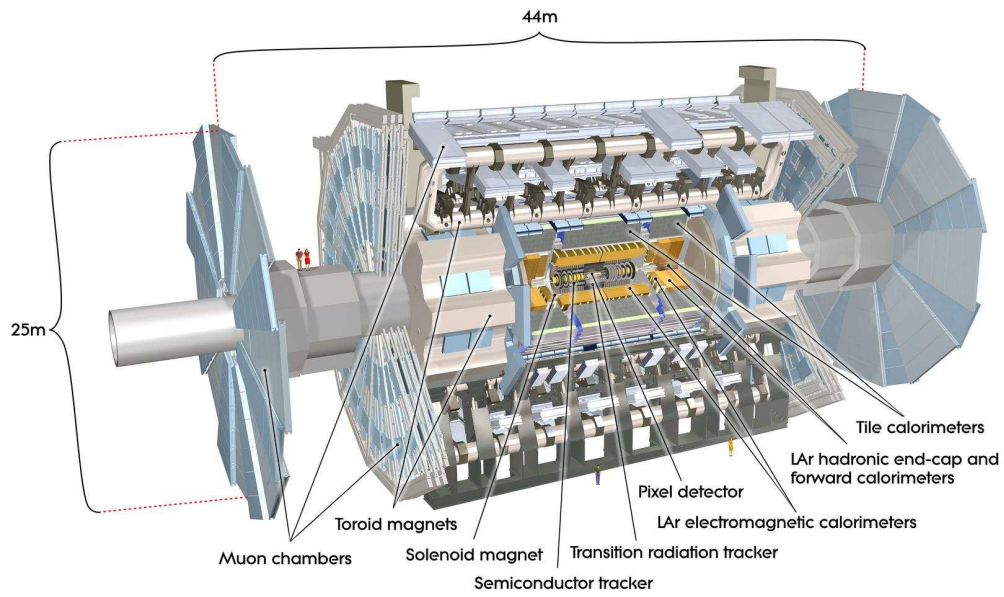


Figure 5.1: Cutaway view of the ATLAS detector, with labels of its major components [1].

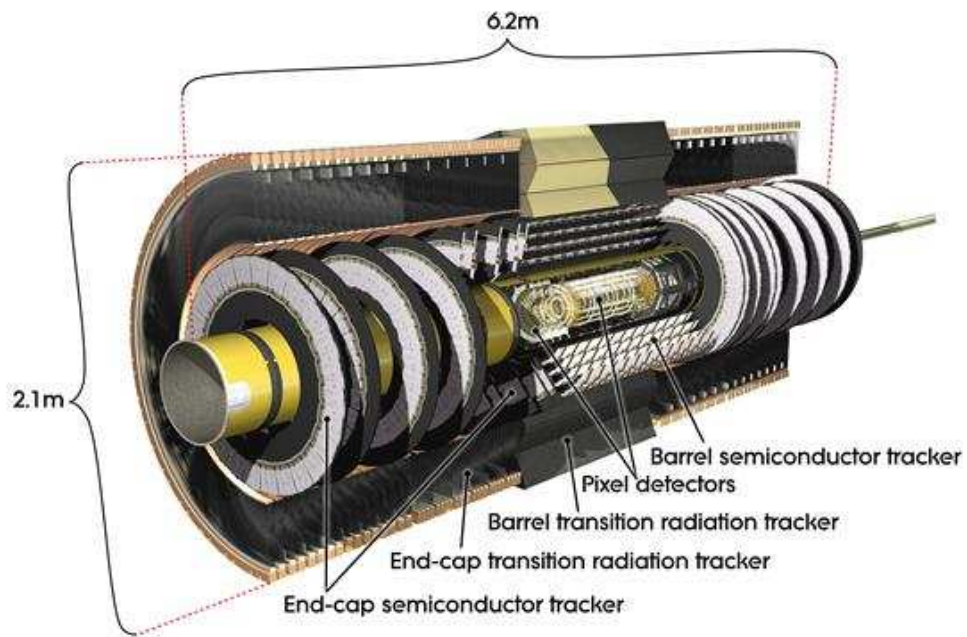


Figure 5.2: Cutaway view of the Inner Detector [1].

5.1 Inner Detector

Just surrounding the interaction point is the Inner Detector, designed to track the path of charged particles moving through the detector. An inner solenoid surrounding the Inner Detector is used to produce a magnetic field of 2 T. This large magnetic field causes the path of charged particles moving through the Inner Detector to bend. Because this magnetic field is uniform and well known, it can be used in conjunction with the curvature of a particle's path to measure its charge and momentum.

The Inner Detector consists of three components - the Pixel Detector, the Semi-Conductor Tracker (SCT), and the Transition Radiation Tracker (TRT). The Pixel Detector is the innermost of these, beginning just 33.25 mm away from the beam line. It consists of three silicon layers along the barrel, as well as three endcap layers, covering a range of $|\eta| < 2.5$.

The Semiconductor Tracker (SCT) is similar to the Pixel detector, but uses long strips rather than small pixels to cover a larger spatial area.

5.2 Calorimeters

Situated outside the Inner Detector are two concentric calorimeters. The inner calorimeter uses liquid argon (LAr) to measure energy of particles that interact electromagnetically, which includes photons and any charged particle. The LAr calorimeter is made of heavy metals, primarily lead and copper, which causes electromagnetically interacting particles to shower, depositing their

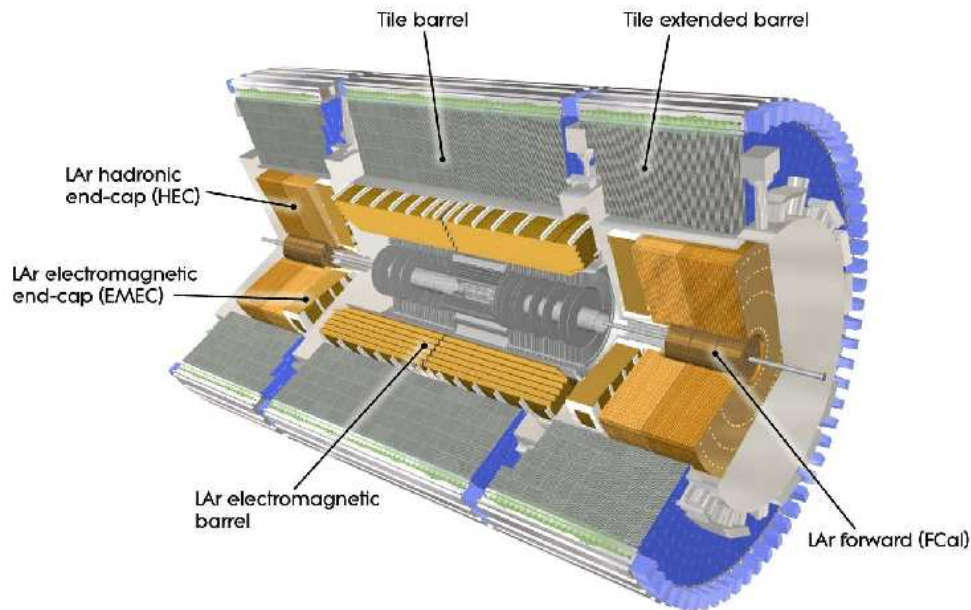


Figure 5.3: Cutaway view of the calorimeter system of the ATLAS detector [1].

267 energy in the detector. The showering of the high energy particles that pass through calorimeter
268 cause the liquid argon to ionize, and the ionized electrons are detected by electronic readouts.
269 The LAr calorimeter consists of around 180,000 readout channels.

270 The outer calorimeter measures the energy from particles that pass through the EM calor-
271 imeter, and measures the energy of particles that interact via the strong force. This is primarily
272 hadrons. It is composed of steel plates to cause hadronic showering and scintillating tiles as the
273 active material. The signals from the hadronic calorimeter are read out by photomultiplier tubes
274 (PMTs).

5.3 Muon Spectrometer

Because muons are heavier than electrons and photons, and do not interact via the strong force, they generally pass through the detector without being stopped by the calorimeters. The outermost components of the detector are designed specifically to measure the energy and momentum of muons produced in the LHC. The muon spectrometer consists of tracking and triggering system. It extends from the outside of the calorimeter system, about a 4.25 m radius from the beam line, to a radius of 11 m. This large detector system is necessary to accurately measure the momentum of muons, which is essential not only for measurements involving the muons themselves, but also to accurately estimate the missing energy in each event.

Two large toroidal magnets within the muon system generate a large magnetic field which covers an area 26 m long with a radius of 10 m. Because the area covered by this magnet system is so large, a uniform magnetic field like the one produced in the Inner Detector is impractical. Instead, the magnetic field that exists in the muon spectrometer ranges between 2 T and 8 T, and is much less uniform. The path of the muons passing through the spectrometer is bent by this field, allowing their charge to be determined.

1200 tracking chambers are placed in the muon system in order to precisely measure the tracks of muons with high spatial resolution.

5.4 Trigger System

Because of the high collision rate and large amount of data collected by the various subdetectors, ATLAS produces far more data than can actually be stored. Each event produces around 25 Mb of raw data, which multiplied by the bunch crossing rate of 40 MHz, comes out to around a petabyte of data every second. The information from every event cannot practically be stored, therefore a sophisticated trigger system is employed in real time to determine whether events are sufficiently interesting to be worth storing.

The trigger system in ATLAS involves multiple levels, each of which select out which events move on to the next level of scrutiny. The level-1 trigger uses hardware information from the calorimeters and muon spectrometer to select events that contain candidates for particles commonly used in analysis, such as energetic leptons and jets. The level-1 trigger reduces the rate of events from 40 MHz to around 100 kHz.

Events that pass the level-1 trigger move to the High-Level Trigger (HLT). The HLT takes place outside of the detector in software, and looks for properties such as a large amount of missing transverse energy, well defined leptons, and multiple high energy jets. Events that pass the HLT are stored and used for analysis. Because the specifics of the HLT are determined by software rather than hardware, the thresholds can be changed throughout the run of the detector in response to run conditions such as changes to pileup and luminosity. After the HLT is applied, the event rate is reduced to around 1000 per second, which are recorded for analysis.

Part IV

Search for Dimension-Six Operators

6 Data and Monte Carlo Samples

This study used data collected by the ATLAS detector over the period from 2015-2018, representing 138.9 fb^{-1} of data at an energy of 13 TeV.

Several Monte Carlo generators were used to simulate both signal and background processes. For all of these, the effects of the ATLAS detector are simulated in Geant4.

7 Object Reconstruction

All analysis channels share a common trigger, jet, and lepton definition.

8 Higgs Momentum Reconstruction

Reconstructing the momentum of the Higgs boson is a particular challenge for channels with leptons in the final state: Because all channels include at least two neutrinos in the final state, the Higgs can never be fully reconstructed. However, the momentum spectrum can be well predicted by a neural network when provided with the four-vectors of the Higgs Boson decay products,

as shown in section 8.1. With this in mind, a sophisticated approach involving several layers of MVAs is used to reconstruct the Higgs momentum.

The first layer is a boosted decision-tree (BDT) algorithm designed to select which jets are most likely to be the b-jets that came from the top decay. The kinematics of these jets are fed into the second layer, also a BDT, which is designed to identify the decay products of the Higgs Boson itself. The kinematics of these particles are then fed into a deep neural-network, which predicts the momentum of the Higgs.

8.1 Truth Level Reconstruction

8.2 b-jet Identification

8.3 Higgs Reconstruction

8.4 p_T Prediction

9 Signal Region Definitions

Events are divided into two channels based on the number of leptons in the final state: one with two same-sign leptons, the other with three leptons.

339 9.1 2lSS

340 9.2 3l

341 10 Background Rejection MVA

342 Various multi-variate analysis techniques (MVAs) are used in order to distinguish signal from
343 background. In particular, BDTs produced with XGBoost are used. Separate MVAs are produced
344 for each of the analysis channels being considered: 2lSS, 3l semi-leptonic, and 3l fully leptonic.
345 Further, because the background composition differs for events with a high reconstructed Higgs
346 p_T compared to events with low reconstructed Higgs p_T , separate MVAs are produced for high
347 and low p_T regions.

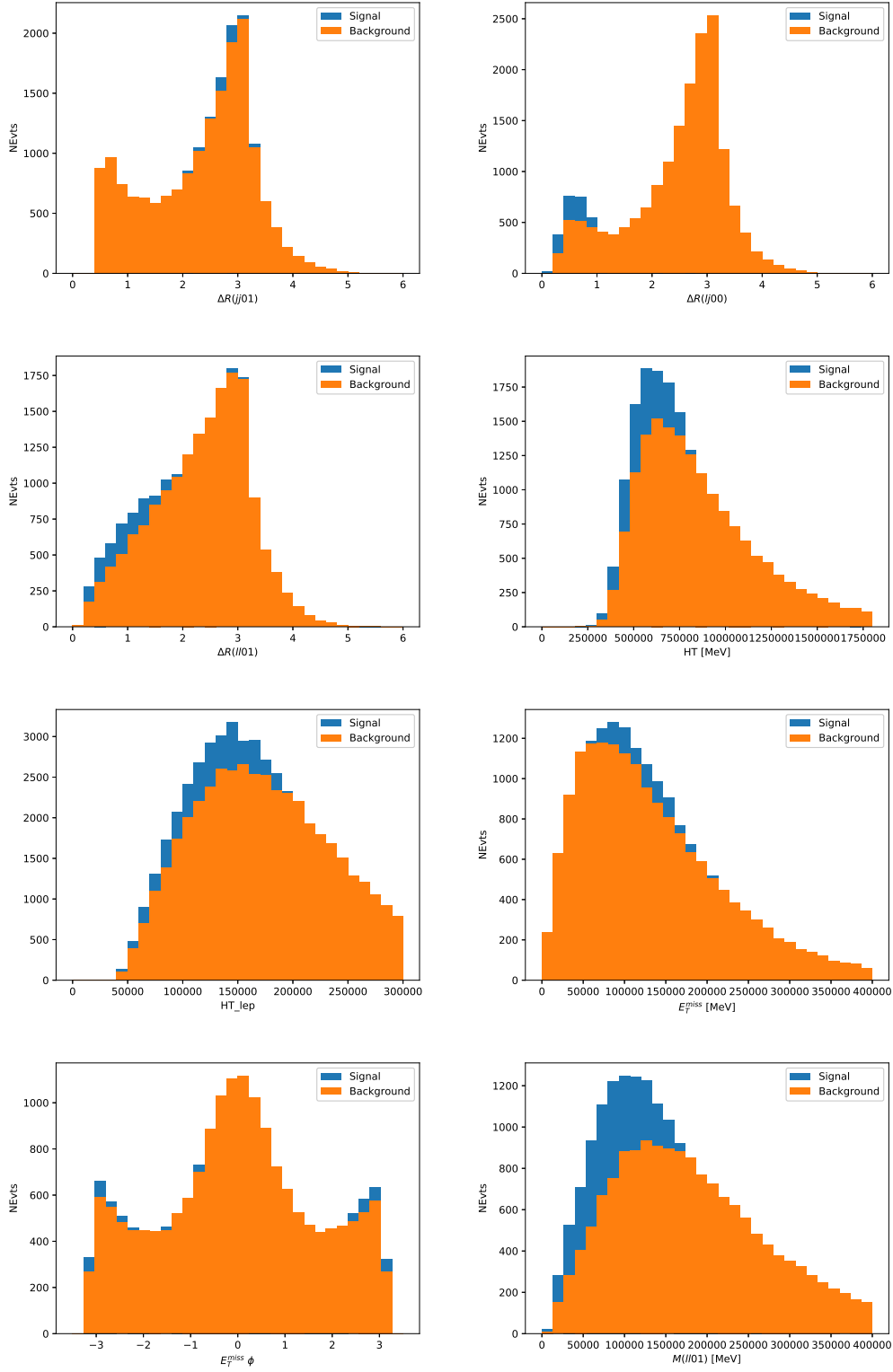


Figure 10.1

348 **10.1 2ISS**

349 **10.1.1 2ISS - High p_T**

350 **10.1.2 2ISS - Low p_T**

351 **10.2 3l Semi-Leptonic**

352 **10.2.1 3l Semi-Leptonic - High p_T**

353 **10.2.2 3l Semi-Leptonic - Low p_T**

354 **10.3 3l Fully Leptonic**

355 **10.3.1 3l Fully Leptonic - High p_T**

356 **10.3.2 3l Fully Leptonic - Low p_T**

357 **11 Systematic Uncertainties**

358 The systematic uncertainties that are considered are summarized in table ???. These are imple-
359 mented in the fit either as a normalization factors or as a shape variation or both in the signal
360 and background estimations. The numerical impact of each of these uncertainties is outlined in
361 section [12](#).

Table 1: Sources of systematic uncertainty considered in the analysis. Some of the systematic uncertainties are split into several components, as indicated by the number in the rightmost column.

Systematic uncertainty	Components
Luminosity	1
Pileup reweighting	1
Physics Objects	
Electron	6
Muon	15
Jet energy scale and resolution	28
Jet vertex fraction	1
Jet flavor tagging	131
E_T^{miss}	3
Total (Experimental)	186
Background Modeling	
Cross section	24
Renormalization and factorization scales	10
Parton shower and hadronization model	2
Shower tune	4
Total (Signal and background modeling)	40
Background Modeling	
Cross section	24
Renormalization and factorization scales	10
Parton shower and hadronization model	2
Shower tune	4
Total (Signal and background modeling)	40
Total (Overall)	226

The uncertainty in the combined 2015+2016 integrated luminosity is derived from a calibration of the luminosity scale using x-y beam-separation scans performed in August 2015 and May 2016 [lumi].

The experimental uncertainties are related to the reconstruction and identification of light leptons and b-tagging of jets, and to the reconstruction of E_T^{miss} . The sources which contribute to the uncertainty in the jet energy scale [jes] are decomposed into uncorrelated components and treated as independent sources in the analysis.

369 The uncertainties in the b-tagging efficiencies measured in dedicated calibration analyses
370 [btag_cal] are also decomposed into uncorrelated components. The large number of components
371 for b-tagging is due to the calibration of the distribution of the BDT discriminant.

372 The systematic uncertainties associated with the signal and background processes are
373 accounted for by varying the cross-section of each process within its uncertainty.

374 12 Results

375 A maximum likelihood fit is performed simultaneously over the regions described in section
376 ??.

377 Part V

378 Conclusion

379 As search for the effects of dimension-six operators on $t\bar{t}H$ production is performed. An effective
380 field theory approach is used to parameterize the effects of high energy physics on the Higgs
381 momentum spectrum. The momentum spectrum is reconstructed using various MVA techniques,
382 and the limits on dimension-six operators are limited to X.

383 **List of contributions**

384

385 **Appendices**

386 **A**